Giant piezoelectricity in fluoropolymer fiber mats achieved by corona poling in water

Guanchun Rui [1], Zhenxing Chen [1], Elshad Allahyarov [2,3,4], Honghu Zhang [5], Ruipeng Li [5], Philip L. Taylor [2,*], and Lei Zhu [1,*]

[1] *Department of Macromolecular Science and Engineering, Case Western Reserve University, Cleveland, Ohio 44106-7202, United States*

[2] *Department of Physics, Case Western Reserve University, Cleveland, Ohio 44106, United States*

[3] *Institut für Theoretische Physik II: Weiche Materie, Heinrich-Heine Universität Düsseldorf, Universitätstrasse 1, 40225 Düsseldorf, Germany*

[4] *Theoretical Department, Joint Institute for High Temperatures, Russian Academy of Sciences, 13/19 Izhorskaya street, Moscow 125412, Russia*

[5] *National Synchrotron Light Source II, Brookhaven National Laboratory, Upton, New York 11973, United States*

* Corresponding authors. Emails: lxz121@case.edu (L. Zhu) and plt@case.edu (P.L. Taylor)

TOC Graphic

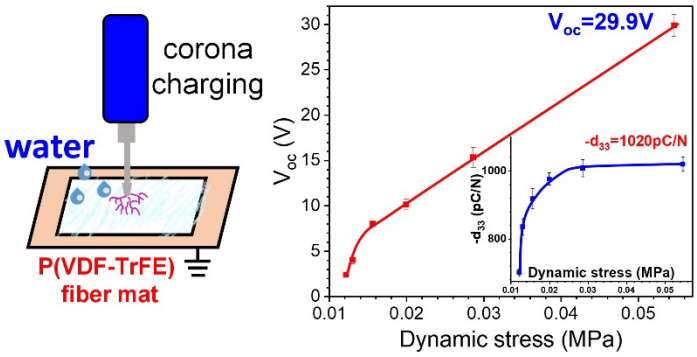
corona
charging
water
P(VDF-TrFE)
fiber mat
V_{oc}=29.9V
$-d_{33}$=1020pC/N
V_{oc} (V)
Dynamic stress (MPa)
$-d_{33}$ (pC/N)
Dynamic stress (MPa)

Abstract

Polymer piezoelectrics hold great potential for energy harvesting and wearable electronics. Efforts have been dedicated to enhancing piezoelectric coefficients and thermostability for several decades, but most of these have not been successful. In this report, we demonstrate a straightforward way to achieve high piezoelectric coefficients and output voltages while maintaining high thermostability at temperatures over 110 °C. Poly(vinylidene fluoride-*co*-trifluoroethylene) [P(VDF-TrFE)] 80/20 mol.% nanofiber mats (made by electrospinning) with extremely high crystallinity and Curie temperatures were obtained via a two-step annealing process, from which large ferroelectric domains were formed in extended-chain crystals. After corona poling using water, which is a high dielectric constant medium, giant piezoelectricity (apparent d_{33} = 1020±20 pC/N) and high output voltages (29.9±0.5 V) were achieved. It is found that the dimensional effect induced significant polarization changes, which is the key requirement for piezoelectricity. Our finding in this work paves a way to further improve high-performance polymer piezoelectrics.

Keywords: Piezoelectric polymers; P(VDF-TrFE); Electrospun nanofiber mats; Corona poling

1. Introduction

Polymer piezoelectrics are of great interest in the fields of wearable sensors, transducers, actuators, and energy harvesters because of their outstanding flexibility and biocompatibility.[1-6] Among all piezoelectric polymers, poly(vinylidene fluoride) (PVDF) and its random copolymers, P(VDF-*co*-trifluoroethylene) [P(VDF-TrFE)], exhibit the best piezoelectric performance (d_{31} and $-d_{33}$ ~ 30 pC/N or pm/V).[5, 7, 8] However, their piezoelectric performance is still much inferior to that of many piezoelectric ceramics. For example, barium titanate shows a strong piezoelectricity, exhibiting a d_{31} of -80 pC/N and a d_{33} of 200-600 pC/N.[9-12] Efforts have been made to further enhance the piezoelectric performance of PDVF-based polymers. These efforts can be mainly divided into two approaches, namely the enhancement of the intrinsic crystal contribution from the morphotropic phase boundary (MPB)[7, 13] and from the extrinsic crystalline-amorphous interface [i.e., the oriented amorphous fraction (OAF)].[8, 14-16] Even though numerous studies have been undertaken on manipulating the polymer structure-property relationship, the piezoelectricity of bulk polymers seems to have reached a plateau.

The origin of piezoelectricity lies in electric polarization changes during the application of a mechanical stress (the direct piezoelectric effect) or dimensional changes during the application of an electrical field (the converse piezoelectric effect). Such polarization changes come from changes in the orientation of individual dipoles or from macroscopic changes in volume and shape. The latter is the so-called dimensional effect, which shows a dominant role in piezoelectric polymers with much lower moduli than those of piezoceramics. The dimensional effect in PVDF-based polymer piezoelectrics was first studied by Wada/Hayakawa[17, 18] and Broadhurst[19, 20] in bulk films in the 1970s. Later, high piezoelectricity was achieved by applying the dimensional effect concept in porous or fibric [e.g., electrospun (ES)] polymer structures.[21-24] In these

materials, the change in dipole moment density or polarization can be many times greater than that of a homogeneous material. However, ES nanofiber mats usually contain numerous defects in ferroelectric domains and weak self-polarization, which limits the piezoelectric performance.

In this work, we demonstrate a convenient method to achieve a high piezoelectric strain coefficient d_{33} and output voltage while maintaining high thermostability at temperatures up to 115 °C. By a rational thermal annealing strategy, a pure ferroelectric phase and extremely high crystallinity were obtained in an ES P(VDF-TrFE) 80/20 mol.% nanofiber mat. Perfect ferroelectric domains in extended-chain crystals (ECCs) are found to be prerequisites for high piezoelectric performance in these nanofiber mats. Then, a non-contact corona poling method in a high permittivity water medium was invoked to efficiently align the ferroelectric domains. Colossal piezoelectricity was subsequently achieved in the P(VDF-TrFE) fiber mats with a piezoelectric coefficient d_{33} of -1020±20 pC/N and an output voltage of 29.9±0.5 V. Moreover, the corona-poled piezoelectric fiber mat in water exhibited strong piezoelectricity up to 115 °C, which is another advantage over many other polymeric piezoelectrics. Our finding demonstrates a simple method to enhance the piezoelectricity of porous hierarchical materials for numerous potential applications.

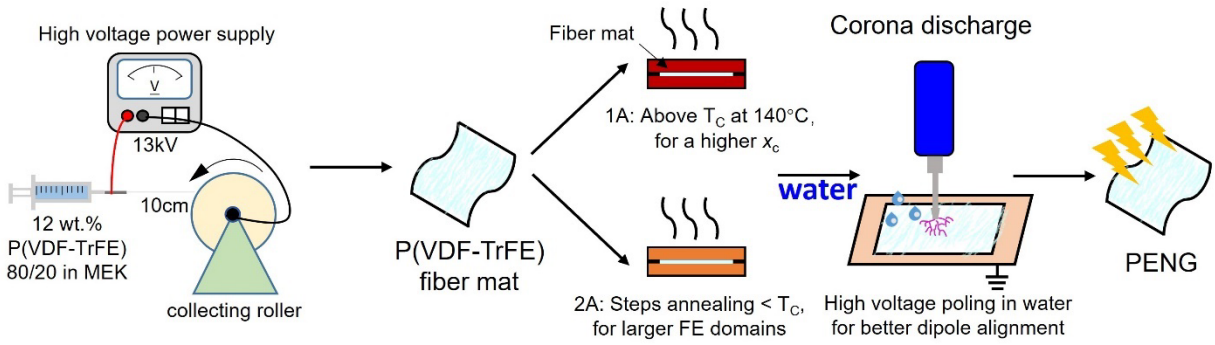

Scheme 1 Schematic representation of the electrospinning and the post corona-poling processes to fabricate the piezoelectric P(VDF-TrFE) 80/20 fiber mat.

2. Results and discussion

2.1. Achieving ECCs with perfect ferroelectric domains via multi-step thermal annealing of P(VDF-TrFE) fiber mats

Using electrospinning equipped with a grounded rolling collector, nonwoven ES fiber mats of P(VDF-TrFE) 80/20 were prepared from 12 wt.% methyl ether ketone (MEK) solution (see Fig. S1 in the Supporting Information). Afterwards, multi-step thermal annealing processes were used to achieve ECCs with perfect ferroelectric domains. Finally, corona-charging was employed to achieve the permanent remanent polarization (P_{r0}) for piezoelectricity. The sample preparation process is shown in Scheme 1.

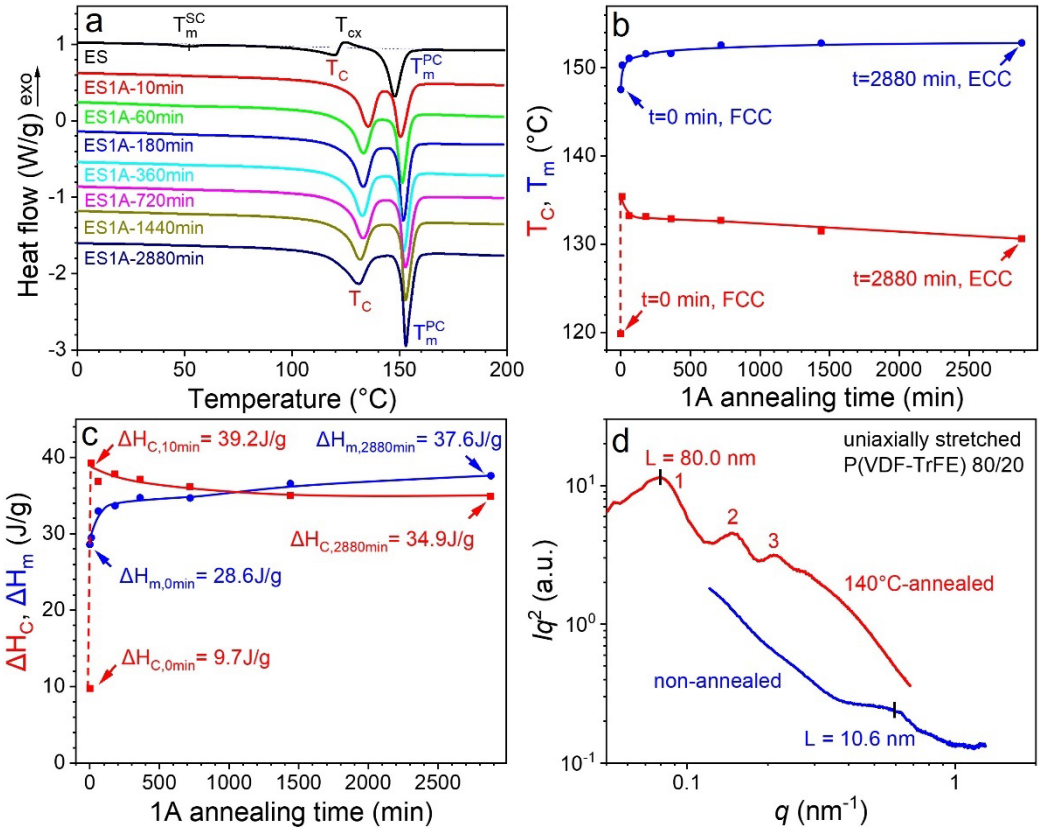

Fig. 1. DSC results for the ES P(VDF-TrFE) 80/20 nanofiber mats annealed at 140 °C for different lengths of time. (a) First-heating curves, (b) T_C/T_m, and (c) $\Delta H_C/\Delta H_m$ as a function of the first annealing (1A) time. (d) Lorentz-corrected SAXS profiles for non-annealed and 140°C-annealed P(VDF-TrFE) 80/20 samples.

In the first thermal annealing (1A) process, the ES fiber mat was held isothermally at 140 °C to produce ECCs via chain-sliding motions in the paraelectric phase, as previously reported.[25-28] Before thermal annealing, the as-spun fiber mat exhibited the melting of secondary ($T_{m,SC}$, heat of fusion $\Delta H_{m,SC}$ = 1.89 J/g) and primary crystals ($T_{m,PC}$) at 51.5 and 147.5 °C, respectively. The Curie temperature (T_C) was observed to be 119.8 °C, followed by a small exothermic peak at 125.1 °C. This peak could be attributed to the cold crystallization (T_{cx}, i.e., crystallization upon heating) from the defect structure frozen during the fast electrospinning process, and it was also reported in a uniaxially oriented P(VDF-TrFE) 75/25 film in a previous publication.[29] The T_C and T_m of the as-spun fiber mat were apparently lower than those of the melt-crystallized sample after removing the memory of thermal history by the first melting (see Fig. S3b later), indicative of defective ferroelectric domains and folded-chain crystals (FCCs) formed during electrospinning.

At 140 °C, a series of isothermal annealing times were chosen: 10, 60, 180, 360, 720, 1440, and 2880 min, and differential scanning calorimetry (DSC) was used to monitor the effect of thermal annealing time on T_C/heat of Curie transition (ΔH_C) and T_m/heat of melting (ΔH_m); see Fig. 1b and 1c. After 10-min of 1A, dramatic changes took place. First, the $T_{m,SC}$ and T_{cx} peaks vanished. As we have discussed before,[15, 30] annealing above $T_{m,SC}$ could melt secondary crystals and recrystallize them onto the prime crystals for P(VDF-TrFE) 80/20, and thus eliminate the T_{cx} peak. Second, improvement of crystalline grains and ferroelectric domains happened simultaneously, and this is reflected by the increase of T_m and $T_C/\Delta H_C$. Upon further 1A annealing, T_m increased to 152.8 °C, and ΔH_m increased to 37.6 J/g at 2880 min. However, the situations for T_C and ΔH_C were different. Namely, after the initial increase, both values slightly decreased with

the extended annealing.

Finally, after 2880-min isothermal annealing at 140 °C, we obtained an ECC structure for P(VDF-TrFE) 80/20 with an extremely high crystallinity (x_c) of almost 80% (ΔH_m= 37.6 J/g, see the powder X-ray data later) and a high T_m of 152.9 °C. The ECC structure was proved by the small-angle X-ray scattering (SAXS) result in Fig. 1d. The overall lamellar thickness (L), which included both crystalline and amorphous layers, increased significantly from 10.6 nm for the non-annealed P(VDF-TrFE) 80/20 to 80.0 nm for the 140°C-annealed sample. During this process, the T_C decreased to 130.6 °C, ΔH_C was 34.9 J/g, and the Curie peak broadened. The decrease in overall Curie transition temperature is due to the thermal annealing higher than T_C. Even though the ferroelectric domain size was decreased, as shown in the Fourier transform infrared result in Fig. S2, no visible conformational defects were generated. All the samples exhibited the all-trans conformation with peaks at 504, 842, and 1284 cm^{-1}.

For semicrystalline homopolymers, the thicker the crystalline lamellar thickness (L_c), the higher the T_m. Their relationship obeys the Gibbs-Thomson equation: $T_m = T_m°(1-K/L_c)$,[31] where $T_m°$ is the equilibrium melting temperature and K is a constant related to the folded-chain surface energy and ΔH_m of 100% ECC. However, it seems that P(VDF-TrFE) 80/20 did not fit well here. As the lamellar thickness L increased about 7.5 times from FCCs to ECCs (see Fig. 1d), the T_m only increased 5.4 °C. We consider that, as the crystalline lamellae thickened, defective segments with more TrFE units were included in the crystalline region, which could decrease both T_m and ΔH_m. Although L_c significantly increased for P(VDF-TrFE) 80/20 upon 1A above the T_C, the experimentally T_m only increased slightly.

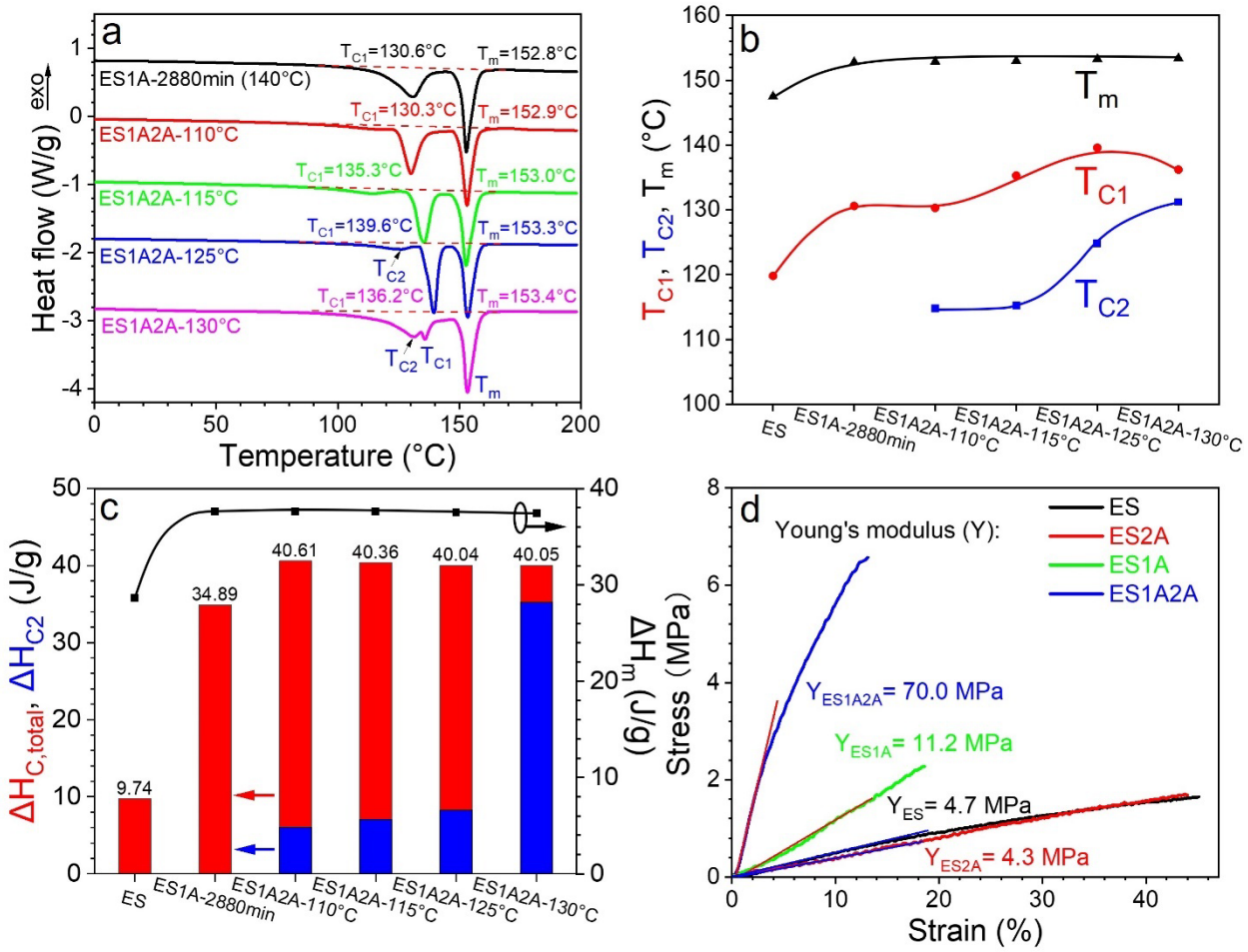

Fig. 2. DSC results of the electrospun P(VDF-TrFE) 80/20 fiber mats after the first annealing (1A) at 140 °C for 2880 min and the second annealing (2A) at different temperatures. (a) First-heating DSC curves. (b) T_{C1}, T_{C2}, and T_m, and (c) $\Delta H_{C,total}$, ΔH_{C2}, and ΔH_m as a function of the 2A temperature. (d) Tensile stress-strain curves for various P(VDF-TrFE) 80/20 fiber mats: ES, ES1A-2880min, ES2A-115°C, and ES1A2A-125°C.

The second annealing (2A) was carried out for ES1A-2880min below T_C with a fixed isothermal time of 1 day to further increase the ferroelectric domain size. Different from PVDF homopolymers, it is proposed that ferroelectric domains in P(VDF-TrFE) could increase their size upon thermal annealing slightly below T_C by enhanced chain-sliding and rotational motions to remove defective domain walls.[25] In the present study, the 2A temperatures were chosen as 110, 115, 125, and 130 °C. As seen in Fig. 2a, two T_C peaks appeared after the second annealing. For example, for the DSC curve of ES1A2A-110°C, the main T_C (T_{C1}) peak was 130.3 °C and the

minor T_C (T_{C2}) was 114.8 °C. The T_{C2} should originate from the "melting" of poor ferroelectric domains at the 2A temperature. When the 2A temperature increased, the primary ferroelectric domains enlarged in size, increasing both T_{C1} and ΔH_{C1} (Fig. 2b). Meanwhile, more "poor" ferroelectric domains "melted", leading to a higher ΔH_{C2}. The T_{C1} reached its maximum value of 139.6 °C upon 2A at 125 °C (Fig. 2b). To quantify the heats of transitions for T_{C1}, T_{C2}, and T_m, Peakfit^{TM} software was used to calculate $\Delta H_{C,total}$, ΔH_{C2}, and ΔH_m (Fig. 2c). It is noteworthy that after 2A at 125 °C, the total $\Delta H_{C,total}$ increased to $\Delta H_{C,total} = \Delta H_{C1} + \Delta H_{C2} = 8.27+31.77$ J/g = 40.04 J/g. The T_{C1} peak height was comparable to the T_m peak height of the paraelectric crystals. To the best of our knowledge, this is the highest ΔH_C value ever achieved for P(VDF-TrFE) random copolymers, suggesting the largest ferroelectric domains achieved by the 2-step thermal annealing, as proposed by Ohigashi and coworkers.[25] In the case of T_m, intriguingly only a slight increase (from 152.8 to 153.3 °C) was seen after 2A at 125 °C. This indicated that the ECC paraelectric crystals were not much affected by the 2A step. Finally, after 2A at 130 °C for ES1A2A-130°C, both T_{C1} and ΔH_{C1} started to decrease, and ΔH_{C2} significantly increased (Fig. 2a-c). This is because the 2A temperature was so high that most ferroelectric domains "melted".

A single-step 2A (i.e., without 1A) was also performed, as shown in Fig. S3a, to compare with the two-step 2A annealing. The highest annealing temperature could only reach 115 °C, and the highest T_C achieved 126.3 °C with a low ΔH_C of 18.1 J/g. After that, a similar "melting" issue of ferroelectric domains was observed. Moreover, the cold crystallization T_{cx} was still observable, and the T_m was only 148.1 °C. These results showed the importance of the 1A step for the 2A to achieve ECCs with large ferroelectric domains in the electrospun fiber mats of P(VDF-TrFE) 80/20.

Tensile mechanical properties of various P(VDF-TrFE) 80/20 fiber mats are presented in Fig. 2d. For the ES and ES2A-115°C fiber mats with FCCs, the Young's modulus (Y) values were

around 4.5 MPa, and the strains at break were around 45%. For the ES1A-2880min fiber mat, ECCs were obtained, and the Y_{ES1A} increased to 11.2 MPa with a decreased strain at break of 18%. Finally, for the ES1A2A-125°C fiber mat with ECCs and the highest crystallinity, the Y_{ES1A2A} increased to 70 MPa while the strain at break further decreased to 13%. The increased Young's modulus and decreased strain at break after extensive thermal annealing should be attributed to the increase crystallinity in the fiber mats.

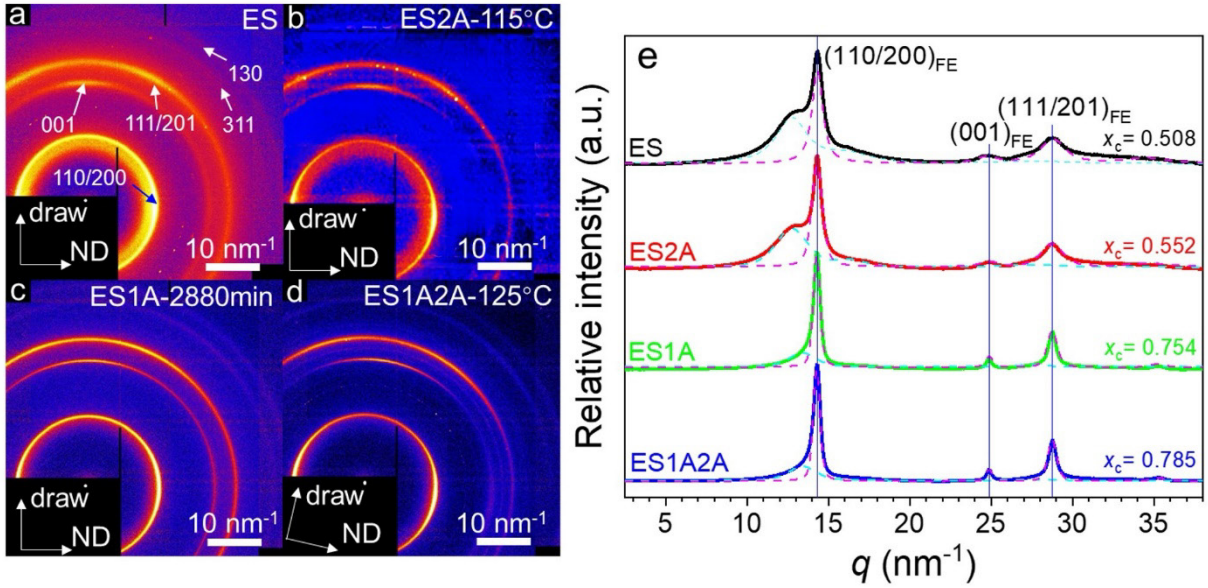

Fig. 3. 2D WAXD fiber patterns for various aligned electrospun P(VDF-TrFE) nanofibers: (a) ES, (b) ES2A-115°C, (c) ES1A-2880min, and (d) ES1A2A-125°C. (e) 1D powder WAXD curves integrated from the 2D patterns in Fig. S5 in the Supporting Information. Crystallinity (x_c) is calculated from peak-fitting, where the cyan dotted curves are the amorphous halo peaks, and the pink dotted curves are the crystalline peaks.

Wide-angle X-ray diffraction (WAXD) was employed to characterize the crystal orientation and crystallinity increase upon thermal annealing. Fig. 3a-d show the 2D WAXD fiber patterns of aligned ES, ES2A-115°C, ES1A-2880min, and ES1A2A-125°C nanofibers, respectively, with the fibers along the vertical direction. The (110/200) reflections of the ferroelectric phase were on the equator, and the (001) reflection was on the meridian. This result

indicated that the ferroelectric crystal *c*-axes (i.e., the chain direction) were oriented along the fiber axis. The 2D powder WAXD patterns of different fiber mats are presented in Fig. S4. From the integrated 1D powder WAXD curves in Fig. 3e, the crystallinity x_c was quantitively determined using the crystalline-amorphous two-phase model:[31] x_c = 0.508 for ES, x_c = 0.552 for ES2A-115°C, x_c = 0.754 for ES1A-2880min (140 °C), and x_c = 0.785 for ES1A2A-125°C. Combining the WAXD x_c of 0.785 and DSC ΔH_m (37.6 J/g) for the ECCs, the ΔH_m of 100% ECC ($\Delta H_m°$) for PV(DF-TrFE) 80/20 was calculated to be 47.9 J/g.

2.2. Suitable testing method to measure piezoelectricity for soft fiber mats

In our recent review article, we have discussed different methods to measure piezoelectricity for solid polymer films.[4] For direct piezoelectricity, the quasi-static method is often used. In this method, the film is applied with a preset static force, on top of which a dynamic force is superposed. The dynamic force can be either a continuous sinusoidal wave [32] or on-off using a weight.[14] The Berlincourt piezo d_{33} meter uses this quasi-static method without the need to measure the sinusoidal polarization output.[32] For direct piezoelectricity measurement, it is important to minimize and subtract triboelectricity.[4] For converse piezoelectricity, a sinusoidal electric field is applied, and the resulting mechanical strain is measured using a fotonic sensor, a linear variable displacement transducer, or a laser interferometer.[4] For highly porous fiber mats, converse piezoelectric measurements usually are not suitable because of the difficulty to implement intimately contacted electrodes onto the porous fiber mat. As such, we can only use the direct piezoelectric measurements. However, the quasi-static method has a deficiency for soft fiber mats. Namely, the static force will compress the fiber mat and significantly reduce the volume. Then, the superposed dynamic force cannot change the volume of the fiber mat to generate

piezoelectric charges anymore. To solve this problem, we used the pure dynamic force method without any static force, and the dynamic force was applied by lifting up and putting down the supporting aluminum rod with a weight. Again, it is important to subtract triboelectric charges to calculate the neat piezoelectric d_{33}. Details should see the Experimental section in the Supporting Information.

2.3. Post corona poling in air and water for enhanced piezoelectricity

After electrospinning, PVDF-based fiber mats exhibit the ferroelectric phase with certain self-polarization because of the high DC voltage applied during electrospinning. The macroscopic P_{r0} orients along the normal direction of the nonwoven nanofiber mat. As a result, the as-ES PVDF-based nanofiber mats often exhibit weak piezoelectricity with a piezoelectric open-circuit voltage (V_{oc}) in the range of 0.2-1.5 V.[33] In this study, the piezoelectric V_{oc} at 0.055 MPa compression was 0.7 V, and the average d_{33} for the as-electrospun nanofiber mat was determined to be -75 pC/N (see Fig. S5).

To further enhance the piezoelectric performance, the above four fiber mats were poled with corona-poling in air at room temperature for 30 min. When these fiber mats were subjected to corona poling in air, it was noticed that the distance between the high-voltage probe and the fiber mat could not be shorter than 2 cm. Otherwise, the high-voltage sparks could burn the top surface of the fiber mats. After corona-poling in air, the apparent d_{33} was determined using direct piezoelectric measurement, as detailed before.[14] The raw data of piezoelectric V_{oc} and charge are presented in Figs. S6 and S7, respectively. For polymer fiber mats, triboelectricity can be generated during compression because of the mechanical contacts/rubbing among different fibers; therefore, it must be subtracted for accurate determination of neat piezoelectricity for fiber mats.

To eliminate the effect of self-polarized P_{r0} in the as-electrospun fiber mats of P(VDF-TrFE) 80/20, the samples were thermally annealed at 140 °C (i.e., above the T_C but below the T_m) for 60 min under a short-circuit condition. Consequently, any aligned dipoles should randomize in individual fibers, and the remanent charges should disappear. Then, triboelectricity was measured directly for the 140 °C-annealed fiber mats, and triboelectric V_{oc} and charge results are shown in Fig. S8. As we can see, both triboelectric V_{oc} and charge increased linearly with the increasing applied dynamic stress.

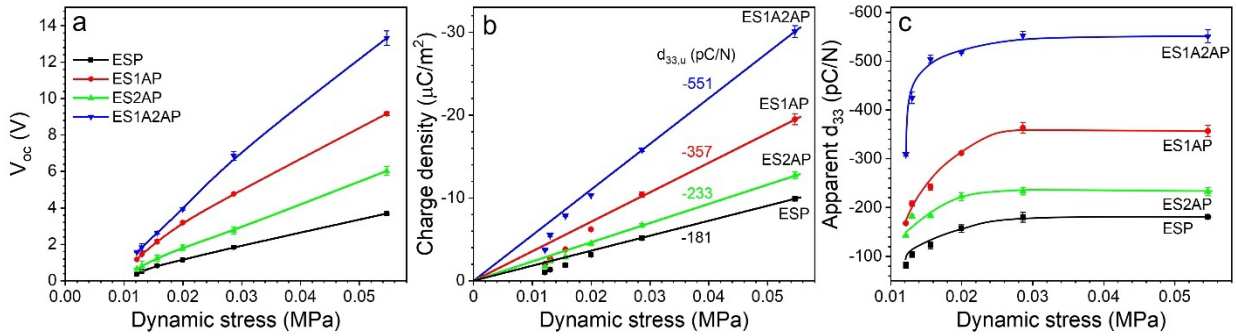

Fig. 4. Piezoelectric (a) V_{oc} and (b) piezoelectric charge density of various ES P(VDF-TrFE) fiber mats with corona-charging in air at room temperature. The ultimate d_{33} ($d_{33,u}$) values from the linear slopes are shown in the plot. (c) Apparent d_{33} values calculated from Eqn. (S1) in the Supporting Information as a function of the dynamic stress.

Fig. 4a,b show piezoelectric V_{oc} and charge density as a function of the dynamics stress for various corona-poled fiber mats in air after subtraction of the triboelectric V_{oc} and charge, respectively. As the dynamic stress increased, both V_{oc} and charge density increased. Here, it is better to avoid using V_{oc} to calculate the apparent d_{33}, because we need to estimate the dielectric constants of the fiber mat under different dynamic stresses, which is not a trivial task (i.e., it is not easy to determine which mixing rule is appropriate). Instead, it is straightforward to use the piezoelectric charge to calculate the apparent d_{33}: $d_{33} = (Q/A_1)/(F/A_2)$, where Q is the piezoelectric charge, A_1 is the electrode area, and F is the applied force on an area A_2. Fig. 4c shows the apparent

d_{33} as a function of the dynamic stress for different nanofiber mats. Before the saturation around 25 kPa, the apparent d_{33} increased with increasing the dynamic stress. Intriguingly, the maximum d_{33} values were closely related to the ECC structure, crystallinity, and ferroelectric domain size (which is inferred from T_C and ΔH_C, see the DSC discussion above). For the corona-poled ES sample (ESP) in air, the maximum -d_{33} was only 181±3 pC/N. This is attributed to its relatively lower crystallinity (50.8%) and small ferroelectric domains (which is reflected by the low T_C of 119.8 °C and the low ΔH_C of 9.7 J/g). For the corona-poled ES1A-2800min sample (ES1AP) in air, the maximum -d_{33} increased to 233±8 pC/N because of its higher crystallinity (75.4%). However, the ferroelectric domain size was still small because of the high annealing temperature of 140 °C above T_C (130.6 °C with ΔH_C = 34.9 J/g). For the corona-poled ES2A-115°C sample (ES2AP) in air, the maximum -d_{33} increased to 357±12 C/N. This is attributed to the increased ferroelectric domain size (T_C = 126.3 °C and ΔH_C = 18.1 J/g). Finally, for the corona-poled ES1A2A-125°C sample (ES1A2AP) in air, the maximum -d_{33} increased to 551±13 pC/N. This is attributed to the thickest ECCs, high crystallinity of 78.5%, and the largest ferroelectric domains (the highest T_C of 139.6 °C and ΔH_C of 40.05 J/g).

Supposedly, the piezoelectric d_{33}, which is a constant, should be obtained from the slope of the linear charge density-dynamic stress curve passing through the origin (see Fig. 4b). This derivation assumes linear relationships in both mechanical and dielectric properties. However, the compression mechanical behavior of fiber mats was nonlinear. Only when the fiber mat was compressed to certain extent (i.e., dynamic stress above 0.025 MPa), the linear mechanical behavior and thus the linear charge density-dynamic stress curve were observed in Fig. 4b. Using this linear lines, the ultimate d_{33} ($d_{33,u}$) values were obtained, as shown in Fig. 4b. As we can see, the apparent d_{33} is different from the ultimate $d_{33,u}$.

During poling in air, the corona-charging with such a long tip-to-sample distance (2 cm) may not be enough to align the P(VDF-TrFE) dipoles well. The dielectric constant of air is very low (ε_r~1) as compared with that of P(VDF-TrFE) (ε_r~10). The electric field will concentrate in the low-permittivity air rather than in the high-permittivity ferroelectric polymer fibers.[34] In addition, massive air breakdowns will cause damage (or even burning) of the fiber mats. Therefore, it is desired to have a liquid or a solid poling medium with a high dielectric constant to further enhance electric poling of dipoles and domains in P(VDF-TrFE) nanofibers. Pure water has a high permittivity of 78.5 at room temperature because of the presence of polar nano-regions,[35] drastically higher than that (~10) of P(VDF-TrFE) 80/20. In the wet nanofiber mat under electric poling, the local electric field inside the low dielectric constant P(VDF-TrFE) nanofibers would be higher than that in the high dielectric constant water medium. The higher local field inside the P(VDF-TrFE) nanofibers could help the poling of ferroelectric domains. Therefore, it can be a good candidate for the post corona poling of P(VDF-TrFE) fiber mats. For the corona-poling in water, we should not use contact-poling, because it is well-known that dipolar water molecules will form an electric double layer (EDL) when it is in direct contact with the metal electrodes.[36] As such, the electric field will concentrate in the very thin EDL (e.g., ca. 2 nm) and cause significant electrolytic reaction at a low applied voltage (~2 V due to the presence of an overpotential). To avoid easy electrolysis, corona-charging of water-wetted fiber mats is chosen for the electric poling, because there is no direct contact between the probe electrode and water. Without the formation of any EDLs, the electric field in the water-wetted fiber mats can be high. Also, we should not use the conventional DC corona poling, which may still be able to degrade water into hydrogen and oxygen gasses to cause fire or explosion. Instead, we choose AC corona poling at 500 kHz to avoid the formation of ionic EDLs and potential electrolytic degradation of

water (see the Experimental section in the Supporting Information). Moreover, the overheating problem can be solved by effective water-cooling, and the distance between the probe and the water-wetted fiber mat can decrease to 0.5 cm without any electric discharge damage. By shortening this distance, the electric field in the wet nanofiber mat is increased, which can further benefit the electric poling of the ferroelectric domains in the P(VDF-TrFE) nanofibers.

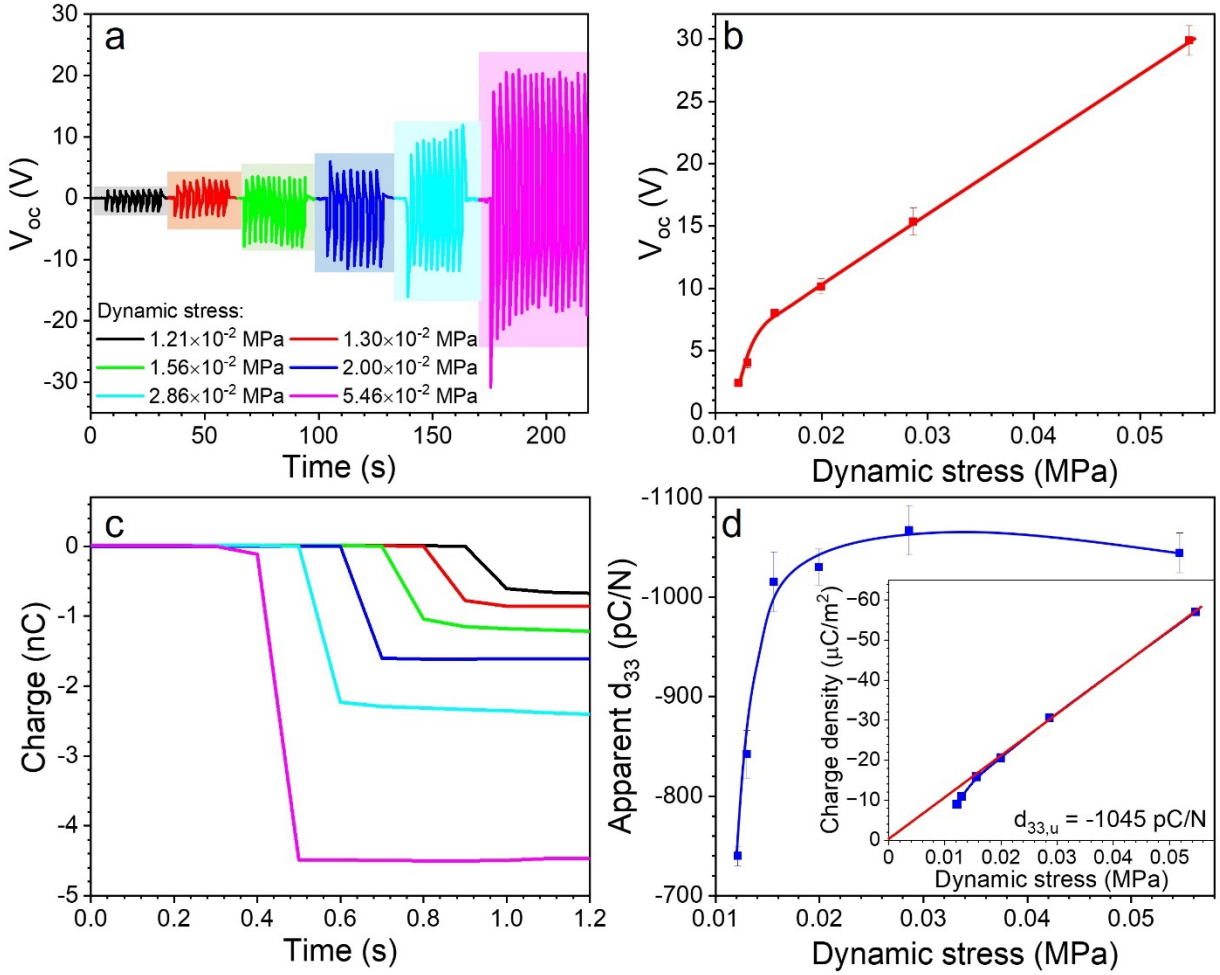

Fig. 5. Piezoelectric performance of the E1A2AP fiber mat corona-charged in water. (a) V_{oc} vs. time under different dynamic stresses, (b) V_{oc} vs. dynamic stress, (c) piezoelectric charge, and (d) apparent d_{33} vs. the dynamic stress. The inset shows the charge density vs. the dynamic stress, from which the ultimate $d_{33,u}$ is calculated to be -1045 pC/N.

Due to the hydrophobic nature of P(VDF-TrFE), direct immersion of the fiber mats in water

would cause many trapped air bubbles. In this study, we used methanol to wet the fiber mats first and then replaced it with water (see Scheme S1). After this procedure, no obvious air bubbles could be observed. After corona-poling in water followed by drying in vacuum, the direct piezoelectric measurement of d_{33} was performed. Figs. 5a,b show the piezoelectric V_{oc} and Fig. 5c shows the piezoelectric charge after subtraction of the triboelectric charge. From the piezoelectric charge density vs. dynamic stress (the inset of Fig. 5d), the apparent d_{33} values were calculated (Fig. 5d). The apparent $-d_{33}$ increased to 1044±20 pC/N when the dynamic stress was above 25 kPa. From the linear charge density-dynamic stress line, the ultimate $d_{33,u}$ was obtained as -1045 pC/N. The output V_{oc} also increased to 29.9±0.5 V (Fig. 5b). To the best of our knowledge, it is one of the highest V_{oc} values achieved for polymer-based piezoelectric energy nano-generators (PENG).

Note that the apparent piezoelectric d_{33} (-1044 pC/N) from the dimensional effect of fiber mats can be significantly larger than the intrinsic limiting d_{33} (ca. -190 pC/N [37]) of solid PVDF or P(VDF-TrFE) samples, which are not really compressible. This is because the fiber mats can be compressed to significantly reduce the volume, thus increasing the apparent d_{33}. The apparent d_{33} of -1044 pC/N for the corona-poled ES1A2A fiber mat in water is comparable to the d_{33} value of -1050 pC/N reported for a solid P(VDF-TrFE)-based tetrapolymer film under a DC bias.[38]

Based on the above experimental observations, the mechanism of corona poling in water to increase the apparent d_{33} could be inferred. First, for corona poling in air, electric field lines will concentrate in air ($\varepsilon_r = 1.0$) and bypass the high dielectric constant ($\varepsilon_r \sim 10$) nanofibers; therefore, the local field in P(VDF-TrFE) nanofibers is very low. Second, for the wet nanofiber mat, electric field lines have to penetrate the condensed nanofiber/water composite film (which has no pores) and the average electric field inside the composite film should become higher. Meanwhile, the dielectric constant ($\varepsilon_r = 78.5$) of water is much higher than that of the nanofibers; therefore, the

local electric field inside the nanofibers should be higher than the average electric field. Meanwhile, we also decrease the air gap distance for the coronal poling in water. This will further increase the local field in the nanofibers. It is the higher local field in the nanofibers during corona poling in water that enhances the electric poling of ferroelectric domains.

2.4. Mechanism of fiber mat piezoelectricity from the dimensional effect

The above piezoelectricity can be explained by the dimensional effect.[18-20] Namely, polarization is defined as: P = M/V, where M is the macroscopic dipole moment in the poled fibers and V is the volume of the fiber mat. As the poled fiber mat is compressed, V shrinks but M keeps constant. As a result, polarization increases to induce direct piezoelectricity (see Scheme S2). In this study, we determined the macroscopic P_{r0} for the corona-poled ES1A2AP fiber mats in air and water ($P_{r0,fm}$). Considering the porosity of the fiber mat, the P_{r0} of the corona-poled P(VDF-TrFE) 80/20 fibers in air and water ($P_{r0,f}$) can be also determined.

In this work, we used an aluminum (Al) rod (130 g) to hold the fiber mat in place, and additional weights (10-500 g) were added on the Al rod to vary the dynamic stress.[4, 14] Both the Al rod and weight were lifted and lowered repeatedly to determine the apparent piezoelectric d_{33}. The dimensional effect, i.e., polarization change (ΔP_n) due to the volume change during the direct piezoelectric measurement, can be quantified as:

$$\Delta P_n = P_n - P_0 = d_{33,n} T_n \quad (1)$$

$$P_n = \frac{M}{V_n} \text{ and } P_0 = \frac{M}{V_0} \quad (2)$$

where P_n is the polarization under a dynamic stress (T_n), and n refers to the experimental run number. For each sample, six weights of 10-500 g were used together with the Al rod, corresponding to six different stresses T_n. V_n is the volume under the specific T_n: $V_n = At_n$, where

A is the sample area under compression (1.04 cm^2), and t_n is the fiber mat thickness. The original volume V_0 was determined from the original thickness t_0 (~ 140 μm) of the free-standing fiber mat, $V_0 = At_0$. In addition, we also measured the thickness changes (Δt_n) of the fiber mat using the MTI 2100 photonic sensor, when different weights were put on the Al rod. Finally, we obtain the following equation:

$$\frac{\Delta Q_n}{A} = \frac{M}{A(t' - \Delta t_n)} - \frac{M}{At_0} = d_{33,n} T_n \quad (3)$$

where ΔQ_n is the piezoelectric charge generated by the dynamic stress T_n (see Fig. 5d). Using nonlinear fitting with Eqn. (3), we determined the macroscopic dipole moment M values, $2.5\pm0.5\times10^{-14}$ and $4.1\pm0.4\times10^{-14}$ C m for corona-poled fiber mats in air and water, respectively. Using the area of 1.04 cm^2 and the original fiber mat thickness of 140 μm, the $P_{r0,fm}$ values of the corona-poled fiber mats air and water were 1.7±0.3 and 2.8±0.3 μC/m^2. Detailed nonlinear fitting is described in Section 7 in the Supporting Information. By measuring the weight of the fiber mat with an area of 1.40×1.40 cm^2, the fiber mat porosity (p) was calculated to be: p = 0.78. Based on the values of M, V_0, and p, the $P_{r0,f}$ values of the corona-poled fiber mats in air and water were determined as 7.5±1.5 and 12.3±1.2 μC/m^2, respectively.

For fully poled P(VDF-TrFE) 80/20 with uniform crystal orientation and 100% crystallinity, the theoretical P_{r0} should be 150 mC/m^2.[39] Assuming a more or less random orientation of the P(VDF-TrFE) nanofibers in the fiber mat and a crystallinity of 75%, the P_{r0} of the fiber should be 1/3×0.75 of the theoretical value: 37.5 mC/m^2. The $P_{r0,f}$ value of 12.7 μC/m^2 for the corona-poled nanofibers in water was significantly lower, suggesting that there should still be much room for further improvement of the piezoelectric performance for the P(VDF-TrFE) 80/20 fiber mats. If a better poling method can be found to further increase $P_{r0,f}$, we could achieve even higher d_{33}.

2.5. Thermal Stability

Comparing PENGs with the triboelectric nanogenerators (TENGs), we see that charges came from the polarization change of the material rather than surface potential. That is, the stability of the PENGs is much better than that of TENGs. Here, we give an example to verify the thermostability of these fiber mat PENGs in Fig. 6. After corona-poling in water, the ES1A2A sample was annealed at different temperatures for 30 min. The piezoelectric measurement was then performed at room temperature to check the remaining piezoelectricity. As shown in Fig. 6a and b, after 30 min thermal annealing, piezoelectricity started to decrease around 100 °C. Above 115 °C, as the T_{C2} (125 °C) was approached, the piezoelectricity sharply decreased. When the annealing temperature was above 140 °C (i.e., the T_{C1}), the piezoelectric effect completely disappeared.

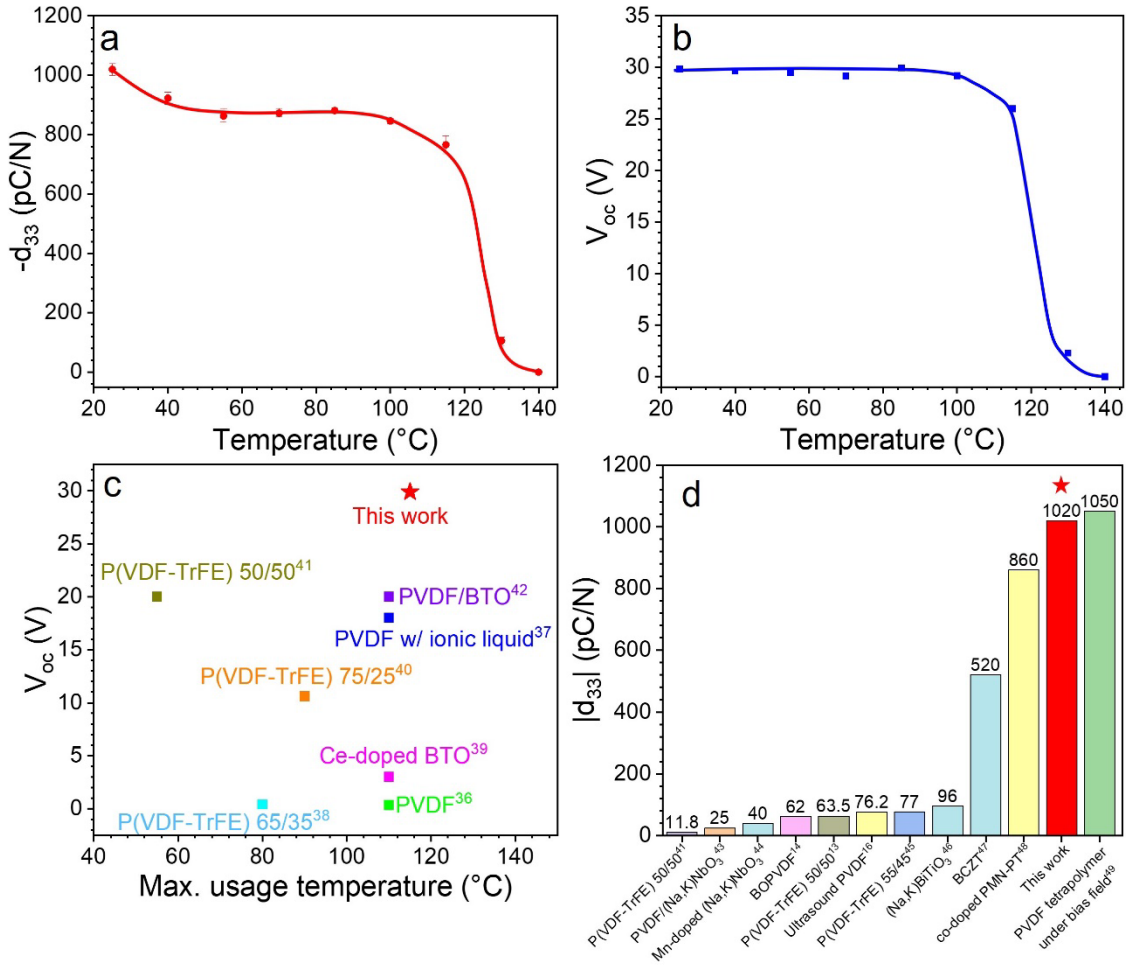

Fig. 6. Piezoelectric performance of the electrospun P(VDF-TrFE) 80/20 nanofiber mat ES1A2A poled with corona discharge in water. The piezoelectric responses: (a) $-d_{33}$ as a function of temperature and (b) V_{oc} as a function of the dynamic stress. Comparison of (c) V_{oc}/maximum usage temperature and (d) apparent $|d_{33}|$ with other electrospun piezoelectric fiber mats and solid piezoelectric films. References ([13, 14, 16, 38, 40-52]) are given as the superscript to sample names in both (c) and (d).

Fig. 6c compares the V_{oc} and maximum usage temperature among different piezoelectric polymers, composites, and $BaTiO_3$. The comprehensive performance of the corona-poled fiber mat in water is summarized in Fig. 6c and 6d, with a comparison with other piezoelectric materials (both fiber mats and solid films) reported in the past. Fig. 6c shows V_{oc} and the thermal stability among different PENGs, and Fig. 6d compares the piezoelectric coefficient $|d_{33}|$ among various piezoelectric materials. From both figures, our corona-poled P(VDF-TrFE) fiber mat in water

showed outstanding performance over most other materials.

3. Conclusion

Utilizing the dimensional effect, we have demonstrated a practical approach to significantly enhance the piezoelectric property of electrospun fiber mats of P(VDF-TrFE) 80/20. Via two-step thermal annealing, large ferroelectric domains and high crystallinity (~80%) were achieved in the ECCs of the P(VDF-TrFE) nanofibers. Non-contact corona poling in both air and water was applied to obtain high piezoelectricity. Intriguingly, a high piezoelectric d_{33} of 1044±20 pC/N and V_{oc} of 29.9±0.5 V was achieved when the fiber mat was poled in a high dielectric constant poling medium of pure water. Moreover, the corona-poled fiber mats in water exhibited high thermostability up to 115 °C, an advance over many other PENGs and TENGs. This method of corona poling in water can be easily extended to other ferroelectric polymer fiber mats, including odd-numbered nylons. This work paves the way to further enhancing piezoelectricity for high-performance polymeric piezoelectrics, which can find potential applications in smart fabrics, wearable energy harvesters, and reusable N95 masks.[5]

Note that the conventional electrospinning method is not suitable for scale-up to mass produce nonwoven piezoelectric fiber mats. However, our method of corona poling in water is not limited to nanofiber mats. Conventional melt-blown fiber mats of ferroelectric polymers should still work when utilizing the dimensional effect for piezoelectricity.

Supporting Information

Supporting Information is available from the Wiley Online Library or from the author.

Acknowledgments

We acknowledge financial support from the National Science Foundation, Division of Materials Research (DMR), Polymers Program (DMR-2103196). E.A. acknowledges financial support from the Ministry of Science and Higher Education of the Russian Federation (State Assignment No. 075-01129-23-00). We thank Daniel Verrico at Case Western Reserve University for help in electrospinning. This research used the 11-BM CMS beamline of the National Synchrotron Light Source II (NSLS-II), Brookhaven National Laboratory (BNL), a U.S. Department of Energy User Facility operated for the Office of Science by BNL under contract DE-SC0012704.

Conflict of interest

L.Z. and G.R. have filed a U.S. provisional patent application (63/597,101) at Case Western Reserve University on piezoelectric fiber mats and the related processing and poling techniques. Otherwise, no additional conflicts of interest to declare.

Data Availability Statement

The data that support the findings of this study are available from the corresponding author upon reasonable request.

References

[1] K.S. Ramadan, D. Sameoto, S. Evoy, A review of piezoelectric polymers as functional materials for electromechanical transducers, Smart Mater. Struct. 23(3) (2014) 033001.

[2] L.F. Brown, Design considerations for piezoelectric polymer ultrasound transducers, IEEE Trans. Ultrason.. Ferroelect. 47(6) (2000) 1377-1396.

[3] W. Yan, G. Noel, G. Loke, E. Meiklejohn, T. Khudiyev, J. Marion, G. Rui, J. Lin, J. Cherston, A. Sahasrabudhe, J. Wilbert, I. Wicaksono, R. Hoyt, A. Missakian, L. Zhu, C. Ma, J. Joannopoulos, Y. Fink, Single fibre enables acoustic fabrics via nanometre-scale vibrations, Nature 603(7902) (2022) 616-623.

[4] L. Zhang, S. Li, Z. Zhu, G. Rui, B. Du, D. Chen, Y. Huang, L. Zhu, Recent progress on structure manipulation of poly(vinylidene fluoride)-based ferroelectric polymers for enhanced piezoelectricity and applications, Adv. Funct. Mater. 33(38) (2023) 2301302.

[5] X. Qian, X. Chen, L. Zhu, Q.M. Zhang, Fluoropolymer ferroelectrics: Multifunctional platform for polar-structured energy conversion, Science 380(6645) (2023) eadg0902.

[6] G.H. Yang, J. Lin, H. Cheung, G. Rui, Y. Zhao, L. Balachander, T. Joo, H. Lee, Z. Smith, L. Zhu, C. Ma, Y. Fink, Single layer silk and cotton woven fabrics for acoustic emission and active sound suppression, Adv. Mater. 36 (2024) 2313328.

[7] Y. Liu, Q. Wang, Ferroelectric polymers exhibiting negative longitudinal piezoelectric coefficient: Progress and prospects, Adv. Sci. 7(6) (2020) 1902468.

[8] G. Rui, E. Allahyarov, Z. Zhu, Y. Huang, T. Wongwirat, Q. Zou, P.L. Taylor, L. Zhu, Challenges and opportunities in piezoelectric polymers: Effect of oriented amorphous fraction in ferroelectric semicrystalline polymers, Resp. Mater. (2024) e20240002.

[9] B. Jaffe, W.R. Cook, H.L. Jaffe, Piezoelectric Ceramics, Academic Press, London, New York, 1971.

[10] T.R. Shrout, S.J. Zhang, Lead-free piezoelectric ceramics: Alternatives for PZT?, J. Electroceram. 19(1) (2007) 113-126.

[11] F. Li, L. Jin, Z. Xu, S. Zhang, Electrostrictive effect in ferroelectrics: An alternative approach to improve piezoelectricity, Appl. Phys. Rev. 1(1) (2014) 011103.

[12] F. Li, L. Wang, L. Jin, D. Lin, J. Li, Z. Li, Z. Xu, S. Zhang, Piezoelectric activity in perovskite ferroelectric crystals, IEEE Trans. Ultrason. Ferroelect. 62(1) (2015) 18-32.

[13] Y. Liu, H. Aziguli, B. Zhang, W. Xu, W. Lu, J. Bernholc, Q. Wang, Ferroelectric polymers exhibiting behaviour reminiscent of a morphotropic phase boundary, Nature 562(7725) (2018) 96-100.

[14] Y. Huang, G. Rui, Q. Li, E. Allahyarov, R. Li, M. Fukuto, G.-J. Zhong, J.-Z. Xu, Z.-M. Li, P.L. Taylor, L. Zhu, Enhanced piezoelectricity from highly polarizable oriented amorphous fractions in biaxially oriented poly(vinylidene fluoride) with pure β crystals, Nat. Commun. 12(1) (2021) 675.

[15] G. Rui, E. Allahyarov, R. Li, P.L. Taylor, L. Zhu, Hard-to-soft transition-enhanced piezoelectricity in poly(vinylidene fluoride) via relaxor-like secondary crystals activated by high-power ultrasonication, Mater. Horizons 9(7) (2022) 1992-1998.

[16] G. Rui, E. Allahyarov, H. Zhang, R. Li, S. Zhang, P.L. Taylor, L. Zhu, Effect of chemical defects on electrostriction-enhanced piezoelectric property of poly(vinylidene fluoride) via high-power ultrasonication, Nano Energy 113 (2023) 108590.

[17] Y. Wada, R. Hayakawa, Piezoelectricity and pyroelectricity of polymers, Jpn. J. Appl. Phys. 15(11) (1976) 2041-2057.

[18] Y. Wada, R. Hayakawa, A model theory of piezo- and pyroelectricity of poly(vinylidene fluoride) electret, Ferroelectrics 32(1-4) (1981) 115-118.

[19] M.G. Broadhurst, G.T. Davis, J.E. Mckinney, R.E. Collins, Piezoelectricity and pyroelectricity in polyvinylidene fluoride - A model, J. Appl. Phys. 49(10) (1978) 4992-4997.

[20] M.G. Broadhurst, G.T. Davis, Physical basis for piezoelectricity in PVDF, Ferroelectrics

60 (1984) 3-13.

[21] J. Chang, M. Domnner, C. Chang, L. Lin, Piezoelectric nanofibers for energy scavenging applications, Nano Energy 1(3) (2012) 356-371.

[22] C. Wan, C.R. Bowen, Multiscale-structuring of polyvinylidene fluoride for energy harvesting: the impact of molecular-, micro- and macro-structure, J. Mater. Chem. A 5(7) (2017) 3091-3128.

[23] Y. Zhang, C.R. Bowen, S. Deville, Ice-templated poly(vinylidene fluoride) ferroelectrets, Soft Matter 15(5) (2019) 825-832.

[24] S. Yu, Y. Tai, J. Milam-Guerrero, J. Nam, N.V. Myung, Electrospun organic piezoelectric nanofibers and their energy and bio applications, Nano Energy 97 (2022) 107174.

[25] M.A. Barique, H. Ohigashi, Annealing effects on the Curie transition temperature and melting temperature of poly(vinylidene fluoride/trifluoroethylene) single crystalline films, Polymer 42(11) (2001) 4981-4987.

[26] H. Ohigashi, K. Omote, T. Gomyo, Formation of single-crystalline films of ferroelectric copolymers of vinylidene fluoride and trifluoroethylene, Appl. Phys. Lett. 66(24) (1995) 3281-3283.

[27] K. Omote, H. Ohigashi, K. Koga, Temperature dependence of elastic, dielectric, and piezoelectric properties of "single crystalline" films of vinylidene fluoride trifluoroethylene copolymer, J. Appl. Phys. 81(6) (1997) 2760-2769.

[28] H. Ohigashi, K. Omote, H. Abe, K. Koga, Chain motions in the paraelectric phase in single crystalline films of vinylidene fluoride and trifluoroethylene copolymer P(VDF/TrFE), J. Phys. Soc. Jpn. 68(6) (1999) 1824-1827.

[29] T. Wongwirat, Z. Zhu, G. Rui, R. Li, P. Laoratanakul, H. He, H. Manuspiya, L. Zhu, Origins

of electrostriction in poly(vinylidene fluoride)-based ferroelectric polymers, Macromolecules 53(24) (2020) 10942-10954.

[30] G. Rui, Y. Huang, X. Chen, R. Li, D. Wang, T. Miyoshi, L. Zhu, Giant spontaneous polarization for enhanced ferroelectric properties of biaxially oriented poly(vinylidene fluoride) by mobile oriented amorphous fractions, J. Mater. Chem. C 9(3) (2021) 894-907.

[31] B. Wunderlich, Macromolecular Physics, Vol. 1: Crystal Structure, Morphology, and Defects, Academic Press, New York, 1973.

[32] A. Barzegar, D. Damjanovic, N. Setter, The effect of boundary conditions and sample aspect ratio on apparent piezoelectric coefficient determined by direct quasistatic method, IEEE Trans. Ultrason. Ferroelect. 51(3) (2004) 262-270.

[33] B. Azimi, M. Milazzo, A. Lazzeri, S. Berrettini, M.J. Uddin, Z. Qin, M.J. Buehler, S. Danti, Electrospinning piezoelectric fibers for biocompatible devices, Adv. Healthc. Mater. 9(1) (2020) 1901287.

[34] K.-C. Kao, Dielectric Phenomena in Solids: with Emphasis on Physical Concepts of Electronic Processes, Elsevier Academic Press, Boston, 2004.

[35] D.C. Elton, M.V. Fernandez-Serra, Polar nanoregions in water: A study of the dielectric properties of TIP4P/2005, TIP4P/2005f and TTM3F, J. Chem. Phys. 140(12) (2014) 124504.

[36] J.O.M. Bockris, A.K.N. Reddy, M.E. Gamboa-Aldeco, Modern Electrochemistry 2A: Fundamentals of Electrodics, 2nd Ed., Kluwer Academic Publishers, New York, 2002.

[37] K. Tashiro, H. Tadokoro, Estimating the limiting values of the macroscopic piezoelectric constants of poly(vinylidene fluoride) form-I, Macromolecules 16(6) (1983) 961-965.

[38] X. Chen, H. Qin, X. Qian, W. Zhu, B. Li, B. Zhang, W. Lu, R. Li, S. Zhang, L. Zhu, F.

Domingues Dos Santos, J. Bernholc, Q. Zhang, Relaxor ferroelectric polymer exhibits ultrahigh electromechanical coupling at low electric field, Science 375(6587) (2022) 1418-1422.

[39] S.M. Nakhmanson, M.B. Nardelli, J. Bernholc, Collective polarization effects in beta-polyvinylidene fluoride and its copolymers with tri- and tetrafluoroethylene, Phys. Rev. B 72(11) (2005) 115210.

[40] R.K. Singh, S.W. Lye, J.M. Miao, Holistic investigation of the electrospinning parameters for high percentage of β-phase in PVDF nanofibers, Polymer 214 (2021) 123366.

[41] H. Asai, Y. Terada, K. Nakane, Effects of the addition of protic organic solvents and the sample formation processes on the crystal structure of poly(vinylidene fluoride): Detailed mechanism of promoting the formation of the β-phase, Polymer 244 (2022) 124650.

[42] L.T. Beringer, X. Xu, W. Shih, W.H. Shih, R. Habas, C.L. Schauer, An electrospun PVDF-TrFe fiber sensor platform for biological applications, Sensor Actuat. A-Phys. 222 (2015) 293-300.

[43] Y. Zhuang, Z. Xu, F. Li, Z. Liao, W. Liu, Improve piezoelectricity and elasticity of Ce-doped $BaTiO_3$ nanofibers - towards energy harvesting application, RSC Adv. 5(68) (2015) 55269-55276.

[44] M. Zhu, S.S. Chng, W. Cai, C. Liu, Z. Du, Piezoelectric polymer nanofibers for pressure sensors and their applications in human activity monitoring, RSC Adv. 10(37) (2020) 21887-21894.

[45] J. Park, Y.W. Lim, S.Y. Cho, M. Byun, K.I. Park, H.E. Lee, S.D. Bu, K.T. Lee, Q. Wang, C.K. Jeong, Ferroelectric polymer nanofibers reminiscent of morphotropic phase boundary behavior for improved piezoelectric energy harvesting, Small 18(15) (2022) 2104472.

[46] Z.-X. Huang, L.-W. Li, Y.-Z. Huang, W.-X. Rao, H.-W. Jiang, J. Wang, H.-H. Zhang, H.-Z. He, J.-P. Qu, Self-poled piezoelectric polymer composites via melt-state energy implantation, Nat. Commun. 15(1) (2024) 819.

[47] M. Kato, K.I. Kakimoto, Processing and energy-harvesting ability of (Na,K)NbO_3 particle-dispersed fibrous polyvinylidene fluoride multilayer composite, Mater. Lett. 156 (2015) 183-186.

[48] H.B. Kang, J. Chang, K. Koh, L.W. Lin, Y.S. Cho, High quality Mn-doped (Na,K)NbO_3 nanofibers for flexible piezoelectric nanogenerators, ACS Appl. Mater. Interface 6(13) (2014) 10576-10582.

[49] Z. Zhu, G. Rui, Q. Li, E. Allahyarov, R. Li, T. Soulestin, F. Domingues Dos Santos, H. He, P.L. Taylor, L. Zhu, Electrostriction-enhanced giant piezoelectricity via relaxor-like secondary crystals in extended-chain ferroelectric polymers, Matter 4(11) (2021) 3696-3709.

[50] Y.Q. Chen, X.J. Zheng, X. Feng, S.H. Dai, D.Z. Zhang, Fabrication of lead-free $(Na_{0.82}K_{0.18})_{0.5}Bi_{0.5}TiO_3$ piezoelectric nanofiber by electrospinning, Mater. Res. Bull. 45(6) (2010) 717-721.

[51] T.K. Jadhav, N.J. Kapadi, A.R. James, V.R. Reddy, R.C. Kambale, Tunable d_{33}/d_{33}^* for MPB $(Ba_{0.85}Ca_{0.15})(Zr_{0.1}Ti_{0.9})O_3$ lead-free piezoceramic by crystallographic texturing approach, Ceram. Int. 50(6) (2024) 9732-9743.

[52] Y. Yang, E. Sun, Z. Xu, H. Zheng, B. Yang, R. Zhang, W. Cao, Sm and Mn co-doped PMN-PT piezoelectric ceramics: Defect engineering strategy to achieve large d_{33} and high Q_m, J. Mater. Sci. Technol. 137 (2023) 143-151.